Stem Cell Reports
Article

ISSCR

OPEN ACCESS

FUS Mutant Human Motoneurons Display Altered Transcriptome and microRNA Pathways with Implications for ALS Pathogenesis

Riccardo De Santis,[1,2] Laura Santini,[2] Alessio Colantoni,[2] Giovanna Peruzzi,[1] Valeria de Turris,[1] Vincenzo Alfano,[2] Irene Bozzoni,[1,2,3] and Alessandro Rosa[1,2,*]

[1]Center for Life Nano Science, Istituto Italiano di Tecnologia, Viale Regina Elena 291, 00161 Rome, Italy
[2]Department of Biology and Biotechnology Charles Darwin, Sapienza University of Rome, P.le A. Moro 5, 00185 Rome, Italy
[3]Institute Pasteur Fondazione Cenci-Bolognetti, Sapienza University of Rome, P.le A. Moro 5, 00185 Rome, Italy
*Correspondence: alessandro.rosa@uniroma1.it
https://doi.org/10.1016/j.stemcr.2017.09.004

SUMMARY

The *FUS* gene has been linked to amyotrophic lateral sclerosis (ALS). FUS is a ubiquitous RNA-binding protein, and the mechanisms leading to selective motoneuron loss downstream of ALS-linked mutations are largely unknown. We report the transcriptome analysis of human purified motoneurons, obtained from *FUS* wild-type or mutant isogenic induced pluripotent stem cells (iPSCs). Gene ontology analysis of differentially expressed genes identified significant enrichment of pathways previously associated to sporadic ALS and other neurological diseases. Several microRNAs (miRNAs) were also deregulated in *FUS* mutant motoneurons, including miR-375, involved in motoneuron survival. We report that relevant targets of miR-375, including the neural RNA-binding protein ELAVL4 and apoptotic factors, are aberrantly increased in *FUS* mutant motoneurons. Characterization of transcriptome changes in the cell type primarily affected by the disease contributes to the definition of the pathogenic mechanisms of *FUS*-linked ALS.

INTRODUCTION

The fatal neurodegenerative disease amyotrophic lateral sclerosis (ALS) is caused by loss of motoneurons (MNs) in the spinal cord and brain, leading to progressive muscle atrophy. Both sporadic ALS (sALS) and familial ALS (fALS) have been linked to a number of genes, including *SOD1*, *C9ORF72*, *TDP-43*, *TAF15*, and *FUS/TLS* (*FUS*) (Renton et al., 2014). The *FUS* gene encodes for an RNA-binding protein involved in RNA biogenesis and maturation (Lagier-Tourenne et al., 2012). Wild-type (WT) FUS is mainly localized in the nucleus, and a hallmark of *FUS* ALS patients is the presence of cytoplasmic inclusions containing mutated protein in the brain and spinal cord (Kwiatkowski et al., 2009; Vance et al., 2009). Many ALS-associated *FUS* mutations disrupt the function of the C-terminal nuclear localization signal (NLS). Therefore, defects in nuclear import, leading to aberrant cytoplasmic localization of FUS, have been proposed as the initial step in ALS pathogenesis (Bentmann et al., 2013; Dormann and Haass, 2011). Recent analyses in murine models suggest that loss of FUS function may not be sufficient to induce MN degeneration (Kino et al., 2015; Scekic-Zahirovic et al., 2016), and both loss of a nuclear function and gain of a toxic function in the cytoplasm have been proposed as contributing pathological mechanisms in *FUS* ALS (Ling et al., 2013).

FUS mutations are expected to exert a major change in the transcriptome. However, this has not been directly addressed in human MNs so far. Human induced pluripotent stem cells (iPSCs) represent a useful system to model ALS, as they can be differentiated into disease-relevant cell types (Sances et al., 2016). iPSCs carrying ALS mutations can be generated by reprogramming from patients (Boulting et al., 2011) or by gene-editing techniques, producing lines that differ only for the specific mutation (Kiskinis et al., 2014; Lenzi et al., 2015). Comparison of gene-edited mutant lines with their otherwise isogenic WT counterparts allows to assign any observed phenotypic difference to the ALS mutation, avoiding any bias due to different genetic backgrounds of non-isogenic mutants and controls.

Recent evidence suggests that microRNAs (miRNAs) might play a role in MN diseases, such as ALS and spinal muscular atrophy (SMA) (Kye and Gonçalves, 2014). Conditional loss of the processing enzyme Dicer in postnatal MNs causes an SMA-like phenotype in mice (Haramati et al., 2010), suggesting that, collectively, miRNAs could be required for MN survival. Global downregulation of miRNAs was observed in MNs of sporadic ALS spinal cords isolated by laser-capture microdissection (Emde et al., 2015), and a protective role for individual miRNAs, such as miR-218 and miR-375, has been shown in MNs (Amin et al., 2015; Bhinge et al., 2016). Previous work from our lab and others has shown that proteins genetically linked to ALS play a role in miRNA biogenesis. FUS stimulates miRNA processing by facilitating the recruitment of the enzyme Drosha on miRNA genes (Morlando et al., 2012), and TDP-43 regulates miRNA biogenesis at multiple levels (Buratti et al., 2010; Di Carlo et al., 2013; Kawahara and Mieda-Sato, 2012). Moreover, overexpression of SOD1, TDP-43, or FUS proteins, either WT or carrying ALS mutations, impaired miRNA processing in the cytoplasm by inducing cellular stress (Emde et al., 2015). As most of the

studies on the contribution of ALS-linked factors to miRNA biogenesis come from cell lines or non-MN cells, it is currently unknown which miRNAs could be affected by ALS mutations in MNs.

Here we took advantage of mutant FUS^{P525L} and isogenic control iPSCs to generate and isolate pure human MNs, which were used for whole-transcriptome analysis by RNA sequencing (RNA-seq). We identified both long and short RNA species significantly altered in *FUS* mutant MNs. Changes in the transcriptome point to pathways previously associated to neurodegenerative diseases, such as those related to cell adhesion. Among differentially expressed miRNAs we focused on miR-375. Levels of miR-375 were decreased in mutant MNs, in which we observed an increase of a subset of its targets, such as p53 and the neural RNA-binding protein ELAVL4. We propose a pathological mechanism in which an impairment of miRNAs production, downstream of *FUS* mutations, would alter RNA metabolism and increase MN vulnerability via aberrant upregulation of pro-apoptotic targets.

RESULTS

Differentiation and Isolation of iPSC-Derived MNs

We have recently reported the generation of iPSC lines devoid of mutations in the *FUS* gene (hereafter FUS^{WT}) or carrying the severe P525L ALS-related mutation introduced by gene editing in both *FUS* alleles (hereafter FUS^{P525L}) (Lenzi et al., 2015). We stably modified these lines by inserting a *Hb9*:GFP reporter into the *AAVS1* locus (Wainger et al., 2014) (Figures S1A and S1B). To improve time and efficiency of MN generation from iPSCs, we took advantage of an optimized protocol based on neural induction and patterning of differentiating cells in adhesion conditions (Figure 1A). Using this protocol we consistently obtained MN progenitors in a 12 day time frame. A time course analysis of marker expression in differentiating FUS^{WT} cells is shown in Figure 1B. By day 6, cells lose the pluripotency marker *NANOG*. Around this time point we detected a peak of expression for the neural progenitor gene *PAX6*, followed by a raise of pan-neuronal (*TUJ1*) and MN (*ISL1*) markers at day 9. The late MN gene *CHAT* was expressed at day 9, with a further increase until day 12. Levels of the MN progenitor marker *HB9* peaked around day 9 and decreased at later time points. The mixed population of differentiated cells at day 12 was highly enriched of *ISL1/2*-positive neurons (Figure S1C). Live cell imaging and flow cytometry analysis indicated that 30%–40% of cells were GFP-positive at this time point (Figures 1C and 1D). Notably, expression of the reporter was detected only in retinoic acid and smoothened agonist (SAG)-treated cells, which induce a ventral spinal cord character, suggesting that the exogenous *Hb9* promoter was correctly turned on in the MN lineage (Figure 1E). We further validated the reporter system by gene expression analysis in distinct cell populations isolated using cell sorting (Figure S1D). Next-generation sequencing (RNA-seq) was performed on total RNA from GFP-positive and -negative cells collected after sorting. Cluster analysis based on gene expression data correctly separated the samples into GFP-positive and -negative ones (Figures S1E and S1F). GFP-positive samples had a similar expression profile, while GFP-negative ones were more dissimilar. A total of 1,631 genes were differentially expressed between GFP-positive and -negative cells, most of them having higher expression levels in GFP-negative samples (Figure S1G; Table S1). As shown in Figure 1F, levels of MN markers (in green) were higher in GFP-positive samples, with the exception of *LHX1*. Notably, the *HB9* transcript was not significantly enriched in GFP-positive samples. This apparent inconsistency can be explained by the narrow window of time of HB9 expression: by the time point in which GFP protein reaches its maximum accumulation (day 12; Figure 1D) the endogenous *HB9* mRNA is already downregulated (Figure 1B). Compared with GFP-positive cells, GFP-negative populations probably contained a fraction of MN progenitors at earlier stages, expressing high levels of *HB9*. As expected, ALS-related genes *SOD1*, *C9ORF72*, *FUS*, and *TARDBP* were not enriched in GFP-positive cells. Experimental validation of selected markers by real-time qPCR confirmed the RNA-seq results (Figure 1G). Purified GFP-positive cells were re-plated on laminin-coated dishes and upon further culturing acquired a neuronal morphology (Figure S1H). Immunostaining analysis indicated that sorted GFP-positive cells were highly enriched for *ISL1/2*-positive MNs (Figure 1H).

Taken together, the combination of a short and efficient differentiation protocol and the stable insertion of the *Hb9*:GFP reporter allowed the effective isolation of a large number of purified, iPSC-derived, MNs.

Transcriptome Profiling in FUS WT and Mutant Human MNs

We have previously shown that ALS mutations in *FUS* do not impair differentiation (Lenzi et al., 2015, 2016). This observation was confirmed in MNs generated with the improved protocol described in Figure 1 from FUS^{WT} and FUS^{P525L} iPSCs. The fraction of GFP-positive cells was consistently comparable over six independent experiments (Figures 2A and 2B). Moreover, GFP-positive cells with a FUS^{WT} or FUS^{P525L} background showed comparable levels of expression of MN markers (Figure S2A). Notably, in the *Hb9*:GFP FUS^{P525L} line both the mutation and the reporter system have been introduced by gene editing. Therefore, besides the FUS^{P525L} mutation, iPSC lines used for subsequent experiments were isogenic.

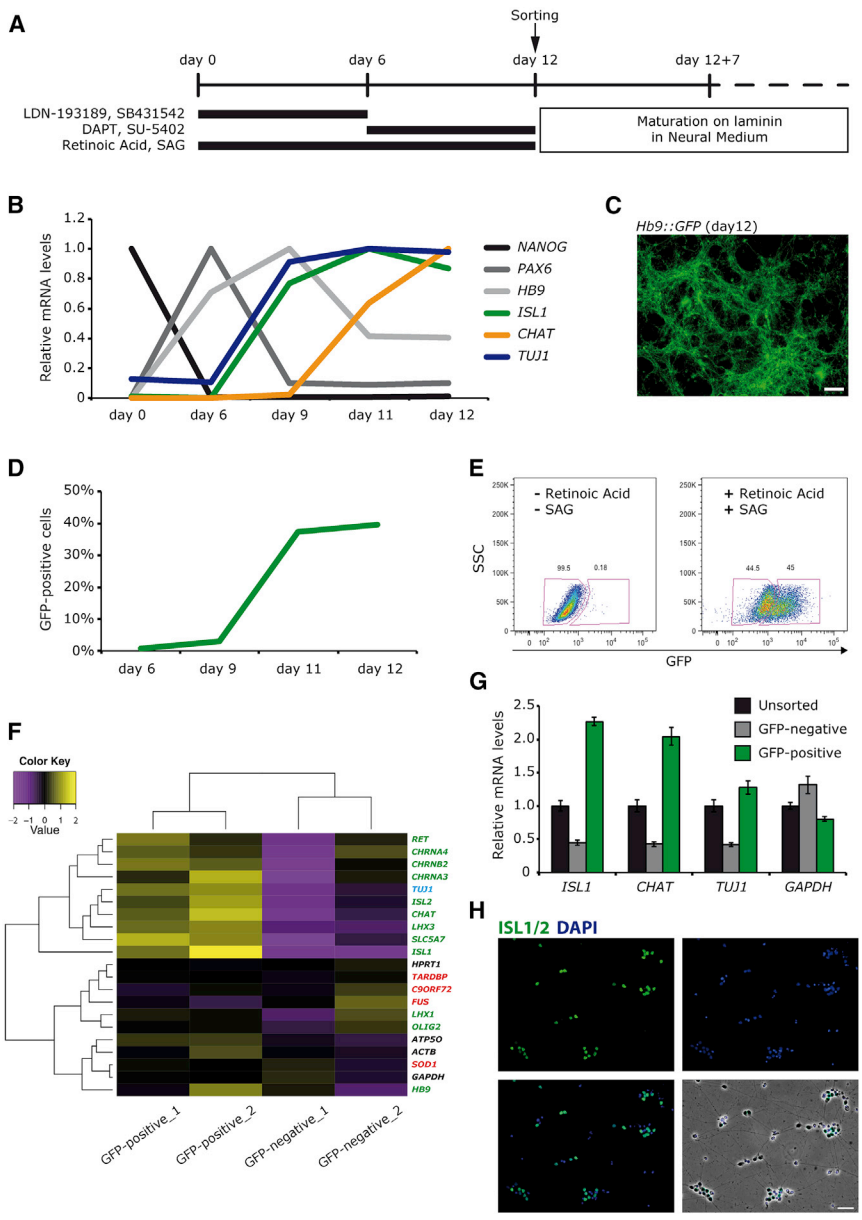

Figure 1. MN Differentiation Protocol and *Hb9*:GFP Reporter

(A) Schematic representation of the differentiation protocol.

(B) Real-time qRT-PCR marker expression analysis. For each marker the time point with the highest expression has been used as the calibrator sample.

(C) Live cell imaging of GFP expression in differentiated cells at day 12. Scale bar, 80 μm.

(D) Schematic representation of flow cytometry analysis of the fraction of GFP-positive cells during differentiation.

(E) Cells were differentiated as in (A) in the presence (right) or in the absence (left) of retinoic acid and SAG, and analyzed by fluorescence-activated cell sorting (FACS) at day 12.

(F) Heatmap representing expression levels of selected genes in sorted GFP-positive and -negative cells (two independent experiments). Plotted values correspond to mean-centered log2-transformed reads per kilobase of transcript per million mapped reads (RPKM) values. MN markers are indicated in green, ALS genes in red, and housekeeping controls in black.

(G) Real-time qRT-PCR analysis of the expression of the indicated genes in unsorted cells (black bars) and GFP-negative (gray bars) and GFP-positive (green bars) cells isolated by FACS (day 12). For each gene the unsorted cells sample has been used as calibrator. Histogram bars represent the average of a technical replicate (n = 3) and error bars indicate the SD.

(H) Immunostaining analysis of sorted MNs (day 12 + 3) with an anti-ISL1/2 antibody (green). Nuclei were stained with DAPI (blue). Upper panels show single channels. Lower panels show merged channels and overlay with the phase contrast image. Scale bar, 40 μm. See also Figure S1.

We took advantage of our iPSC system to systematically analyze the consequences of the FUS^{P525L} mutation on the transcriptome in pure populations of *in-vitro*-derived human MNs. GFP-positive FUS^{WT} and FUS^{P525L} iPSCs were sorted at day 12 of differentiation and further cultured on laminin-coated dishes for an additional 7 days (day 12 + 7). Total RNA from three independent differentiation experiments was collected and analyzed by RNA-seq. Gene expression-based cluster analysis resulted in the segregation of samples into two distinct groups based on their *FUS* genotype (Figures S2B and S2C). Out of 14,289 genes expressed in human MNs, 267 genes were upregulated and 244 downregulated in a consistent manner in FUS^{P525L} compared with FUS^{WT} (false discovery rate [FDR] < 0.05) (Table S1). The gene expression heatmap of differentially expressed genes is shown in Figure 2C. RNA-seq results were validated by real-time qPCR in at least three additional independent samples. Figure 2D shows validation of four representative genes among those downregulated (*SCL17A8*, *NXPH2*, *CRIM1*, and *GRIN2A*) and upregulated (*TP53I3*, *CDH7*, *NNAT*, and *TSPYL5*). Expression of the *FUS* transcript itself, as well as the mRNAs of other major

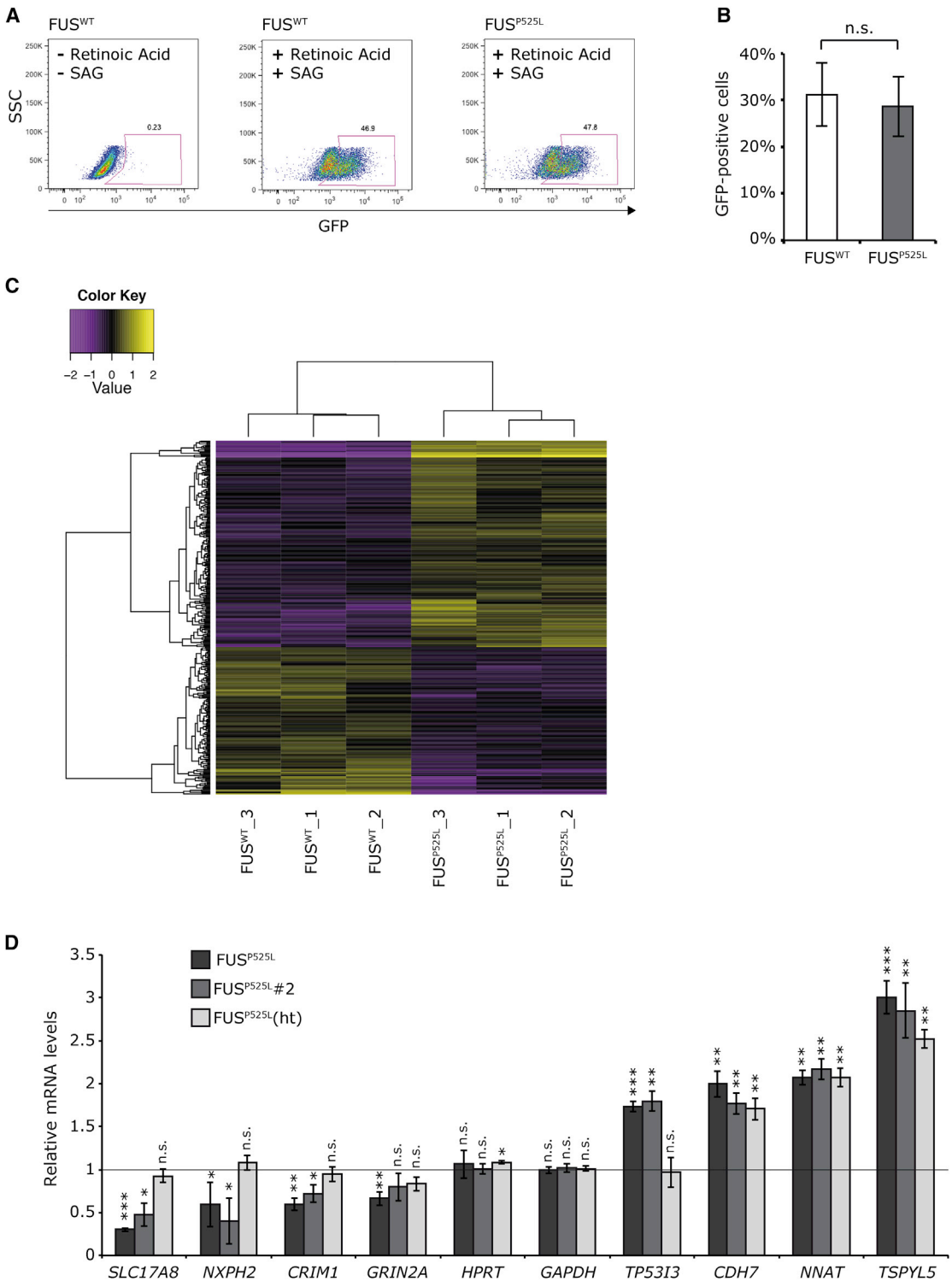

Figure 2. RNA-Seq Analysis of FUS^{WT} and FUS^{P525L} iPSC-Derived MNs

(A) Representative FACS plots of FUS^{WT} and FUS^{P525L} cells at day 12. As a negative control, FUS^{WT} cells were differentiated in the absence of retinoic acid and SAG (left panel).

(B) Schematic representation of flow cytometry analysis (day 12). Histogram bars represent the average of six independent experiments and error bars indicate the SD (Student's t test; unpaired; two tails; n.s., $p > 0.05$).

(legend continued on next page)

ALS-related genes, was not significantly altered in *FUS* mutant MNs (Figure S2D).

We confirmed these results in an independent *FUS* WT and mutant isogenic pair. A second FUS^{P525L} iPSC line (hereafter FUS^{P525L}#2), generated as previously described (Lenzi et al., 2015), and its parental FUS^{WT} iPSC line (hereafter FUS^{WT}#2) were modified by inserting the *Hb9*:GFP reporter into the *AAVS1* locus (Figures S3A–S3D). FUS^{WT}#2 and FUS^{P525L}#2 were then differentiated, sorted, and collected at day 12 + 7 for RNA analysis. All genes analyzed in the original isogenic pair resulted consistently altered in MNs obtained from these new iPSC lines (Figure 2D).

A subset of these genes was also affected in MNs obtained from a *Hb9*:GFP-modified heterozygous FUS^{P525L} iPSC line, hereafter FUS^{P525L}(ht) (Lenzi et al., 2015) (Figure 2D).

Functional Consequences of the FUS^{P525L} Mutation in Human MNs

We next assessed whether the change in the transcriptome detected in *FUS* mutant cells might be informative of pathways potentially involved in ALS MN degeneration. Gene ontology (GO) term enrichment analysis with the FIDEA tool (D'Andrea et al., 2013) highlighted relevant categories that cooperate in pathways and distinct molecular functions. In particular, we noticed a striking enrichment for categories related to cell adhesion in genes differentially expressed in FUS^{P525L} MNs (Figure 3A). Notably, "cell adhesion" is one of the categories consistently enriched in multiple studies focusing on FUS-bound transcripts and splice targets in mouse and human neurons (Orozco and Edbauer, 2013). GO term enrichment analysis of differentially expressed genes in laser-captured MNs from postmortem sporadic ALS patients also indicated "cell adhesion" (Batra et al., 2016). Moreover, functional enrichment analysis for genome-wide association studies involving several neurological diseases (including ALS) showed significant values for the "cell-cell adhesion" GO category (Guio-Vega and Forero, 2017). This category was also enriched in the analysis of differentially expressed genes in ALS fibroblasts carrying the *C9ORF72* mutation (Kotni et al., 2016). Cell adhesion-related categories were enriched also when upregulated and downregulated genes were analyzed separately (Figure S4A). Interestingly, the Kyoto Enrichment of Genes and Genomes pathway "Neuroactive ligand-receptor interaction" was specifically enriched by the downregulated genes. Previous work found this pathway enriched in RNA profiling from *C9ORF72* mutant fibroblasts (Kotni et al., 2016) and linked to neurological diseases such as Parkinson's disease (Kong et al., 2015).

Seeking for ALS signature in *FUS* mutant MNs, we crossed our RNA-seq data with a recently published dataset from laser-captured MNs fom sALS patients (Batra et al., 2016; Kapeli et al., 2016). In these works, the authors found 2,346 upregulated and 955 downregulated genes in sALS patients. The variation of upregulated genes was more robust, since more stringent selection criteria had lower impact on their abundance. These two lists of genes were employed as two distinct gene sets in the context of a gene set enrichment analysis to evaluate whether they were over-represented in the set of genes deregulated upon *FUS* mutation. Notably, the set of genes downregulated in sALS patients was enriched among those downregulated in FUS^{P525L} (FDR = 0.151), and the set of genes upregulated in sALS patients was significantly enriched among those upregulated in FUS^{P525L} (FDR = 0.009) (Figure S4B). These results suggest a common signature in gene expression between *in-vitro*-derived FUS^{P525L} MNs and sALS MNs. As suggested by FDR values, this tendency is stronger for the upregulated genes, consistent with the robustness of their deregulation in sALS patients.

We next investigated whether there is any relationship between differential gene expression and direct FUS binding in mutant MNs. The FUS interactome has never been characterized in purified human MNs; however, FUS CLIP-seq (crosslinking and immunoprecipitation, followed by high-throughput sequencing) data from human brain cortex are available (Lagier-Tourenne et al., 2012). We reanalyzed this dataset and evaluated the position of FUS binding clusters relative to the different regions of the pre-mRNAs, which are expressed in our MNs. FUS binding was enriched in the exonic regions of protein-coding genes, and in particular in the 3′ UTR, when compared with sequences located more (distal introns) or less (proximal introns) than 500 bp from the nearest exon-intron junction (Figure 3B). FUS-bound genes were classified as differentially expressed or not in FUS^{P525L} MNs, and individual mRNA regions were analyzed separately. A significantly higher percentage of genes modulated in FUS mutant MNs was directly bound by FUS in the distal intron and 3′ UTR (Figure 3C). When the same analysis was repeated with the TDP-43-bound genes dataset (Tollervey et al., 2011), we did not observe a significant enrichment

(C) Heatmap representing RNA-seq-derived expression levels of differentially expressed genes at day 12 + 7 (three independent experiments). Plotted values correspond to mean-centered log2-transformed RPKM values.

(D) Validation of selected genes by real-time qRT-PCR in MNs at day 12 + 7. Expression levels in FUS^{P525L}, FUS^{P525L}#2, and FUS^{P525L}(ht) are shown as relative to their respective isogenic FUS^{WT} controls, set to a value of 1. Histogram bars represent the average of at least three independent experiments and error bars indicate the SD (Student's t test; paired; two tails; *p < 0.05; **p < 0.01; ***p < 0.001; n.s., p > 0.05). See also Figures S2 and S3.

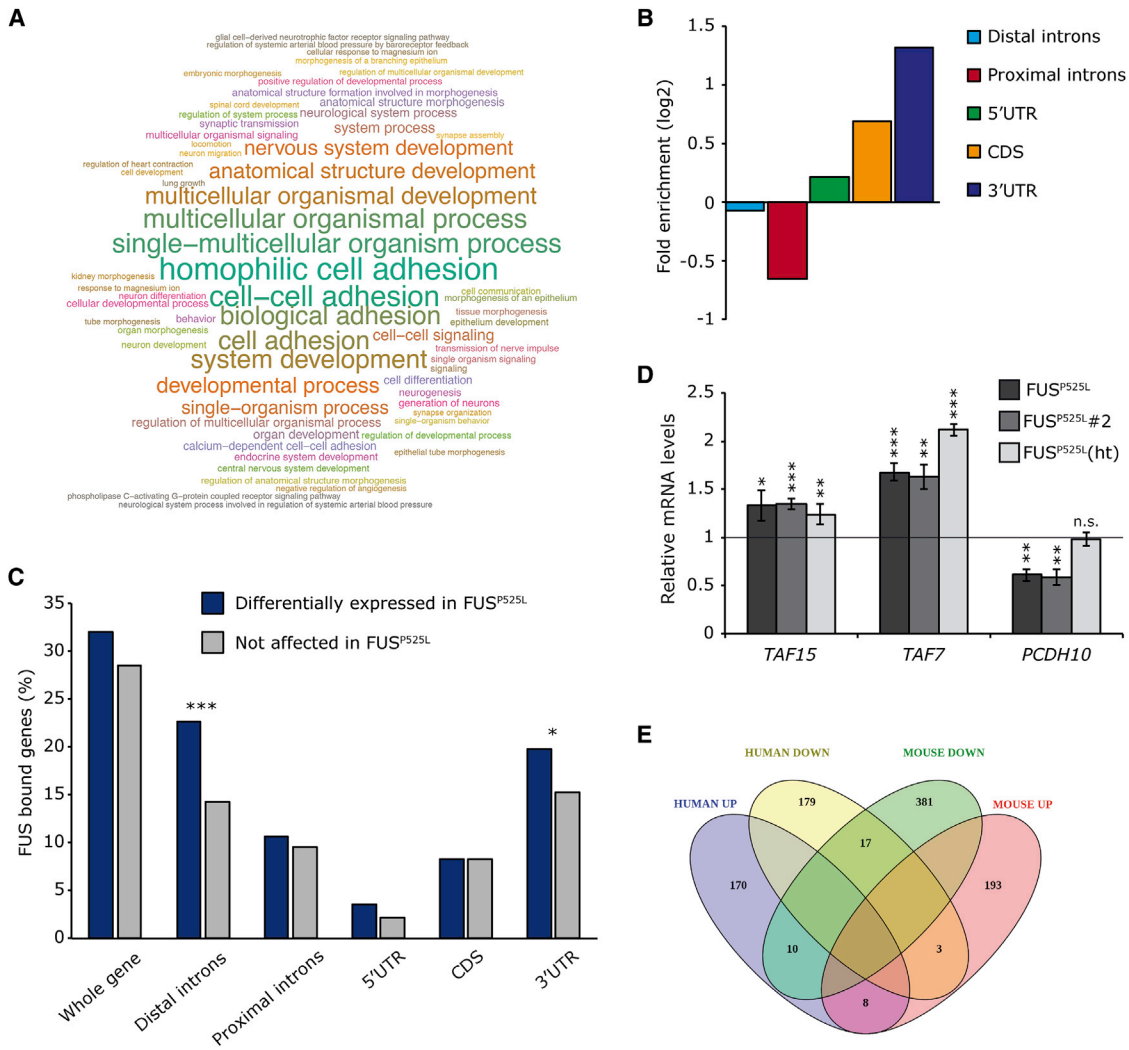

Figure 3. Bioinformatics Analysis of Differentially Expressed Genes in FUS^{WT} and FUS^{P525L} MNs

(A) Word cloud generated by FIDEA representing GO biological process terms enriched in the list of genes that are differentially expressed between FUS^{WT} and FUS^{P525L} MNs. The functional categories are represented with a character size proportional to the statistical significance of their enrichment.

(B) The histogram shows the fold enrichment of FUS binding sites, identified by re-analysis of data from Lagier-Tourenne et al. (2012), in different regions of pre-mRNAs, after normalization to average region size.

(C) Fraction of FUS bound protein-coding genes, which are also differentially expressed genes in FUS mutant MNs. A gene was considered bound if a FUS HITS-CLIP peak was found within its body; the analysis was repeated focusing only on specific pre-mRNA regions (Fisher's exact test; *p < 0.05; ***p < 0.001).

(D) Validation of selected FUS-bound genes in MNs at day 12 + 7 by real-time qRT-PCR. Expression levels in FUS^{P525L}, FUS^{P525L}#2, and FUS^{P525L}(ht) are shown as relative to their respective isogenic FUS^{WT} controls, set to a value of 1. Histogram bars represent the average of at least three independent experiments and error bars indicate the SD (Student's t test; paired; two tails; *p < 0.05; **p < 0.01; ***p < 0.001; n.s., p > 0.05).

(E) Venn diagram showing the overlap between differentially expressed genes in the present work and in a FUS mutant mouse (Scekic-Zahirovic et al., 2016). See also Figure S4.

for the 3′ UTR set (Figure S4C). Taken together, these results suggest that mRNAs bound by FUS in the 3′ UTR might be more susceptible to changes in FUS activity due to ALS mutations. We validated differential expression of selected FUS-bound mRNAs in mutant MNs (*TAF7*, *TAF15*, *GRIN2A*, *PCDH10*, and *CRIM1*) (Figures 2D and 3D).

To assess whether the changes in gene expression downstream of *FUS* ALS mutations are consistent with an animal

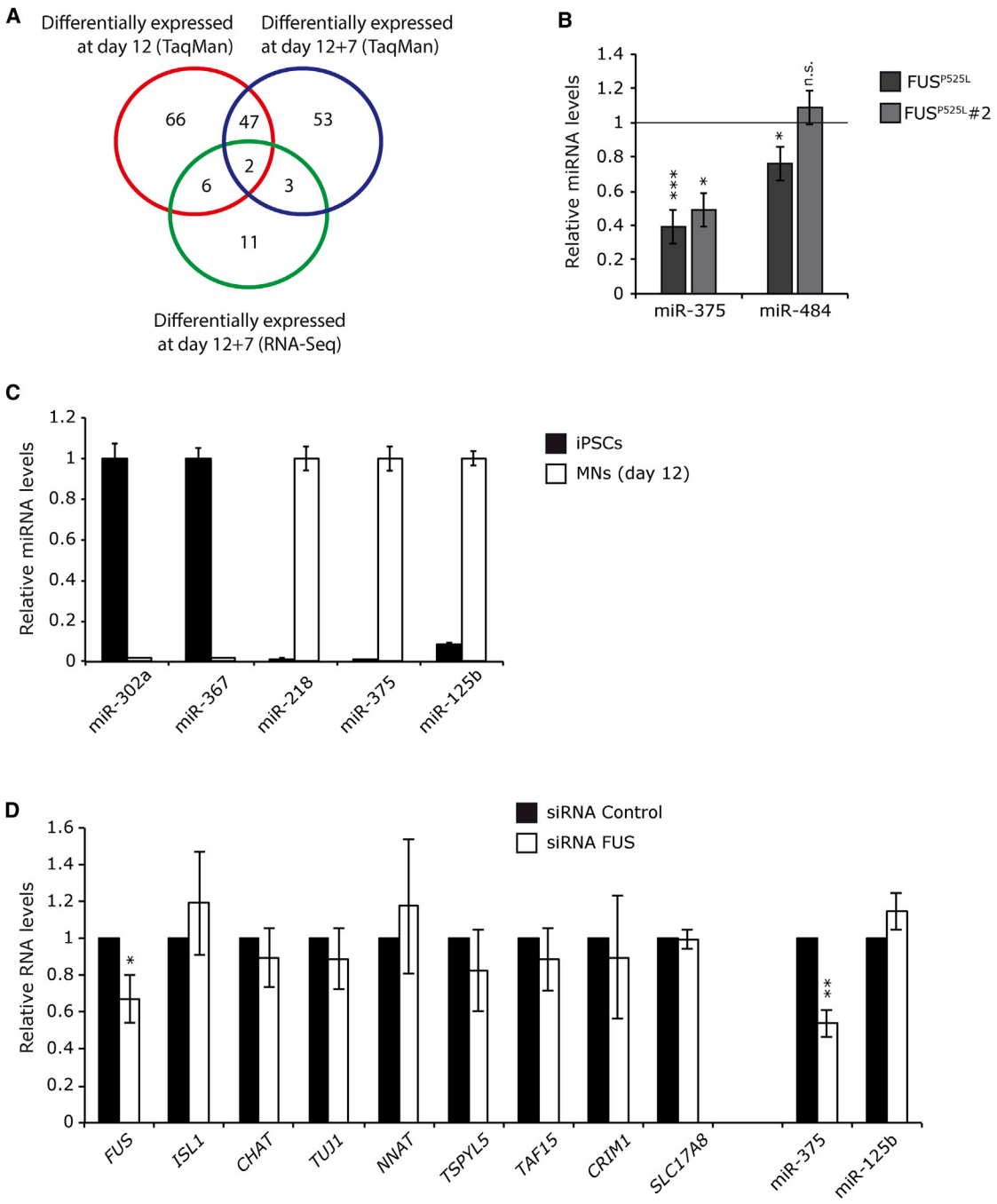

Figure 4. miR-375 Is Downregulated in FUS Mutant MNs

(A) Venn diagram showing the relations between differentially expressed miRNAs at different time points of MN maturation, as resulting from TaqMan array cards analysis in FUS^{WT} and FUS^{P525L} iPSC-derived MNs at day 12 and 12 + 7, and small RNA-seq at day 12 + 7 ($p < 0.05$).

(B) Validation of selected miRNAs by real-time qRT-PCR in MNs at day 12 + 7. Expression levels in FUS^{P525L} and FUS^{P525L}#2 are shown as relative to their respective isogenic FUS^{WT} controls, set to a value of 1. Histogram bars represent the average of at least four independent experiments and error bars indicate the SD (Student's t test; paired; two tails; *$p < 0.05$; ***$p < 0.001$; n.s., $p > 0.05$).

(C) Real-time qRT-PCR analysis of the indicated miRNAs in FUS^{WT} undifferentiated iPSCs and MNs (day 12 of differentiation, unsorted). miR-302a and miR-367 are pluripotency miRNAs; miR-218 is an MN-enriched miRNA. For each miRNA, the sample with the highest

(legend continued on next page)

model exhibiting ALS features, we crossed our data with the transcriptome profiling of a recently described mouse carrying targeted deletion of the PY-NLS ($Fus^{\Delta NLS/\Delta NLS}$) (Scekic-Zahirovic et al., 2016). This mutation severely impairs the nuclear localization of FUS, mimicking the human P525L mutation and other truncations of the protein C-terminal. Among differentially expressed genes, 17 were downregulated and 8 were upregulated in both mutant mouse brain and human MNs (Figures 3E and S4D). The overlap was statistically significant both for upregulated and downregulated gene lists (p value for hypergeometric test <0.05). Interestingly, mRNA levels of *TAF15*, a *FUS* family member mutated in a subset of fALS patients (Couthouis et al., 2011), were significantly increased in both mouse (Scekic-Zahirovic et al., 2016) and human (Figure 3D). *TAF15* was among the transcripts directly bound by FUS (Lagier-Tourenne et al., 2012). These findings suggest that a possible crosstalk between *FUS* and *TAF15*, hypothesized in murine models, might be conserved in human.

FUS^{P525L} Mutation Impairs miR-375 Biogenesis in MNs by a Loss-of-Function Mechanism

Previous studies in cell lines have hypothesized a link between *FUS* mutations and the impairment of miRNA function (Emde et al., 2015; Morlando et al., 2012), but this was never directly investigated in human MNs. We performed miRNA profiling by small RNA sequencing (small RNA-seq) in FUS^{WT} and FUS^{P525L} MNs. Based on miRNA expression levels, samples could be clustered according to their *FUS* genotype (Figures S5A–S5C). Of the 573 miRNAs expressed in human MNs (day 12 + 7), 21 resulted downregulated and 11 upregulated in FUS^{P525L} mutant cells (FDR < 0.05) (Figure S5D; Table S1). We also analyzed to which extent the change in the miRNome is maintained at different time points. TaqMan array cards and small RNA-seq identified miR-375 and miR-484 as differentially expressed miRNAs at both day 12 and day 12 + 7 (Figure 4A; Table S2). These and other selected candidates were analyzed by real-time qRT-PCR in FUS^{P525L}, FUS^{P525L}#2, and FUS^{P525L}(ht) MNs, and their isogenic WT controls (Figures 4B, S5E, and S5F). Among them, miR-375 was consistently downregulated in both homozygous *FUS* mutant lines over at least four independent experiments (Figure 4B).

miR-375 has been recently described as a protective miRNA in MNs (Bhinge et al., 2016). Consistent with previous observations (Bhinge et al., 2016), miR-375 was highly upregulated in MNs compared with undifferentiated iPSCs (Figure 4C). To gain insights into the mechanisms underlying miR-375 downregulation in FUS^{P525L} MNs we transfected differentiating FUS^{WT} iPSCs with small interfering RNAs (siRNAs) targeting *FUS* and analyzed gene expression at day 12 of differentiation. In these conditions, *FUS* levels were reduced to about 60% compared with scramble siRNA-transfected cells (Figure 4D). We have previously shown that FUS localization in the nucleus in homozygous FUS^{P525L} cells is reduced to 50% of its normal levels, due to partial delocalization in the cytoplasm (Lenzi et al., 2015). Therefore, the decrease of FUS achieved by siRNA in WT cells is expected to reproduce possible loss of nuclear function effects of the mutation. FUS reduction did not affect differentiation, as assessed by *ISL1*, *CHAT*, and *TUJ1* marker analysis (Figure 4D). Levels of miR-375 were significantly reduced upon FUS knockdown (Figure 4D). Conversely, expression of selected genes among the most upregulated (*NNAT*, *TSPYL5*, and *TAF15*) or downregulated (*CRIM1* and *SLC17A8*) ones in FUS^{P525L} MNs was not affected by FUS knockdown (Figure 4D).

These results suggest that ALS mutations in the *FUS* gene might impair miR-375 production via a nuclear loss-of-function mechanism, while gain of toxic functions of the mutated protein might underlie the alteration of protein-coding genes expression.

miR-375 Target Genes in *FUS* Mutant MNs

To identify miR-375 targets in human MNs, we crossed mRNA expression data from the RNA-seq with predicted (TargetScan; Agarwal et al., 2015) and previously validated targets (miRTarBase; Chou et al., 2016). Eight mRNAs upregulated in FUS^{P525L} MNs were also miR-375 predicted targets (Figure 5A; Table S3), including *ELAVL4* (also known as *HuD*), which had been previously validated as a *bona fide* miR-375 target (Abdelmohsen et al., 2010). The increased expression of *ELAVL4* and other predicted targets (*PHLDA1*, *EBF3*, *B3GAT2*) in mutant MNs was validated by real-time qPCR (Figure 5B). The *ELAVL4* gene encodes for a neuron-specific RNA-binding protein (Bronicki and Jasmin, 2013). In mouse MNs, the transcript of the *NRN1* (*CPG15*) gene is among known targets of ELAVL4, which promotes *NRN1* mRNA accumulation by enhancing its stability (Akten et al., 2011). In line with this, we detected increased levels of *NRN1* in FUS^{P525L} MNs (Figure 5B).

We then noticed that the p53 gene (*TP53*) was a previously described target of miR-375 (Liu et al., 2013). *TP53* mRNA was unchanged or slightly upregulated,

expression has been used as the calibrator. Histogram bars represent the average of a technical replicate (n = 3) and error bars indicate the SD.

(D) Real-time qRT-PCR analysis in differentiated FUS^{WT} iPSCs (day 12) transfected with anti-FUS or control siRNAs. Histogram bars represent the expression relative to the siRNA control (average of three independent experiments). Error bars indicate the SD (Student's t test; paired; two tails; *p < 0.05; **p < 0.01; where not indicated p > 0.05). See also Figure S5.

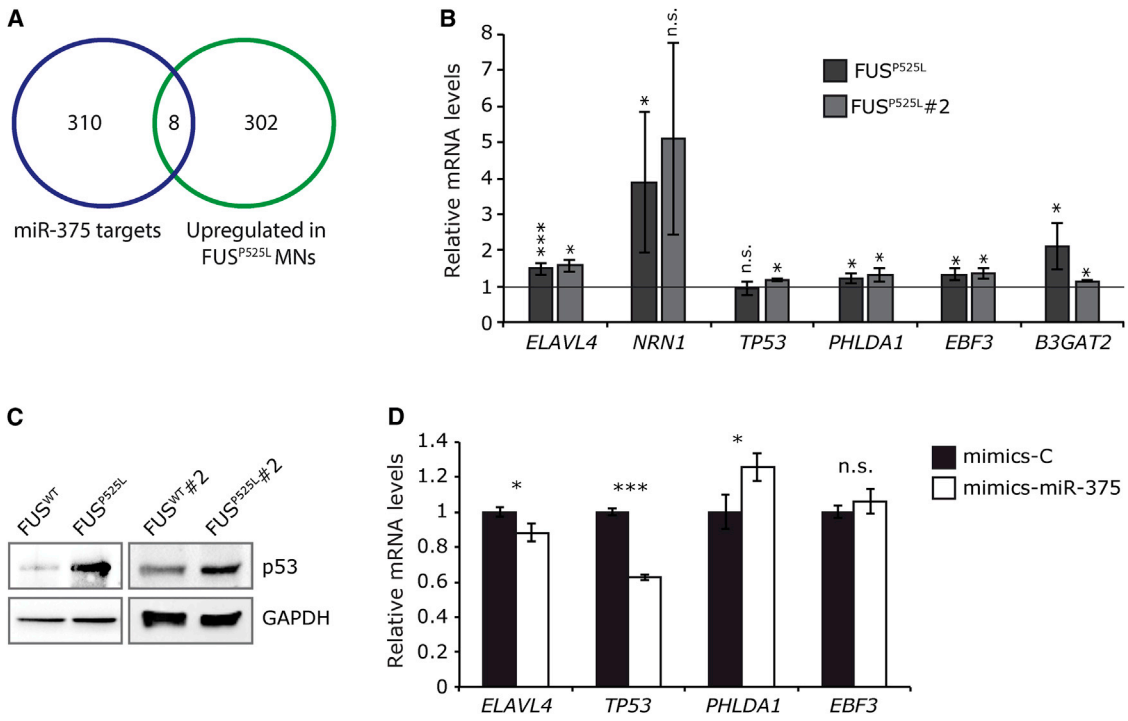

Figure 5. miR-375 Target Analysis

(A) Venn diagram showing the relations between predicted miR-375 targets and mRNAs upregulated in FUS^{P525L} MNs, as resulting from the RNA-seq analysis.

(B) Real-time qRT-PCR analysis in MNs at day 12 + 7. Expression levels in FUS^{P525L} and FUS^{P525L}#2 are shown as relative to their respective isogenic FUS^{WT} controls, set to a value of 1. Histogram bars represent the average of at least three independent experiments and error bars indicate the SD (Student's t test; paired; two tails; *p < 0.05; ***p < 0.001; n.s., p > 0.05).

(C) Western blot analysis of p53 protein levels in FUS wild-type and mutant MNs at day 12 + 7. GAPDH is used as a housekeeping control.

(D) Real-time qRT-PCR analysis of the expression of the indicated genes in differentiated FUS^{P525L} iPSCs transfected with miR-375 miRNA mimics. Expression levels are relative to mimics control (mimics-C)-transfected samples. Histogram bars represent the average of at least three independent experiments and error bars indicate the SD (Student's t test; paired; two tails; *p < 0.05; ***p < 0.001; n.s., p > 0.05).

respectively, in FUS^{P525L} and FUS^{P525L}#2 MNs (Figure 5B). In both lines, we detected an increase of p53 protein by western blot (Figure 5C). Among miR-375 targets, we noticed that *EBF3* and *PHLDA1* (also known as *TDAG51*) have been previously involved in the induction of apoptosis (Gomes et al., 1999; Zhao et al., 2006).

To assess whether changes in target mRNA levels could be explained by differences in miRNA levels, we transfected synthetic miR-375 mimics in FUS^{P525L} differentiated cells. We observed a significant decrease of *ELAVL4* and *TP53* mRNA levels compared with control-transfected cells (mimics-C) (Figure 5D). Since levels of *EBF3* and *PHLDA1* were not decreased, we hypothesize that other mechanisms might contribute to their upregulation in FUS mutant cells.

Collectively, these findings suggest that dysregulation of miR-375 in *FUS* mutant MNs may have an impact on RNA metabolism and survival due to aberrant increase of ELAVL4 and p53, respectively.

DISCUSSION

In this study we report the whole-transcriptome profile of *in-vitro*-derived human MNs with WT or mutant (P525L) *FUS* background. Our analysis was performed on two pairs of isogenic lines generated by gene editing. We therefore provide significant information on the changes in the transcriptome of the neuronal subtype primarily affected by ALS and due solely to the specific, ALS-linked, FUS^{P525L} mutation. This represents a major advance beyond previous work, in which the transcriptome of mixed populations of progenitor cells (composed for the most part of non-MN cells and derived from non-isogenic *FUS* control/mutant iPSCs) was profiled by exon array (Ichiyanagi et al., 2016).

We found that numerous differentially expressed genes belong to functional categories related to the cell adhesion pathway. Interestingly, this correlates with transcriptome analysis of postmortem laser-capture microdissected MNs

from ALS patients, genome-wide association studies on several neurological diseases and differential gene expression in *C9ORF72* mutant cells (Aronica et al., 2015; Batra et al., 2016; Guio-Vega and Forero, 2017; Kotni et al., 2016). In the light of our findings, cell adhesion-related pathways might be considered as biomarkers and/or therapeutic targets in *FUS* ALS patients.

We also crossed our data with the transcriptome analysis from a recently reported murine model (Scekic-Zahirovic et al., 2016). Among genes commonly upregulated in both species we noticed *TAF15*, which is mutated in some ALS patients (Couthouis et al., 2011). TAF15 is a member of the FET family of RNA-binding proteins and is closely related to FUS. Similarly to FUS and TDP-43, upregulation of WT TAF15 causes neurodegeneration in *Drosophila* (Couthouis et al., 2011). Notably, *TAF15* levels were slightly increased in FUS null mice (Kino et al., 2015; Scekic-Zahirovic et al., 2016), but not in human MNs with reduced FUS levels (Figure 4D). This discrepancy might be explained by residual FUS protein in our RNAi experiment. A shift in TAF15 solubility and its localization into FUS-positive inclusions has been observed in frontotemporal lobar degeneration, but not in ALS (Neumann et al., 2011). Therefore, it remains unclear whether TAF15 upregulation in FUS mutant MNs contributes to ALS pathogenesis.

Changes in mRNA levels may be a direct consequence of the *FUS* mutation. Despite the fact that specific information on FUS-bound transcripts in human MNs is still missing, FUS CLIP-seq data from human brain cortex are available (Lagier-Tourenne et al., 2012). Our results suggest a possible direct effect of *FUS* mutations on those transcripts that are targeted by FUS on their 3′ UTR. Interestingly, levels of several transcripts were altered in the same direction in homozygous and heterozygous FUS^{P525L} MNs. The P525L mutation is inherited in an autosomal dominant way in ALS patients, and homozygous individuals have never been reported. Unexpectedly, in spinal cord tissue from heterozygous *FUS* ALS patients a near absence of nuclear FUS was observed in MNs, suggesting that both mutant and WT FUS can be sequestered within cytoplasmic inclusions (Vance et al., 2013). As the nuclear fraction of FUS in homozygous and heterozygous P525L cells is, respectively, 80% and 50% (Lenzi et al., 2015), the homozygous mutant could be regarded as representative of a more advanced stage of the disease. Mechanistically, toxic functions of mutant FUS might underlie the alteration of at least a subset of mRNAs, as suggested by knockdown experiments.

FUS mutations might also affect gene expression indirectly, for instance by altering miRNA levels. We found that miR-375 levels were consistently lower in MNs derived from two independent FUS^{P525L} lines. Bhinge et al. (2016) recently showed that miR-375 is enriched in human spinal MNs derived from embryonic stem cells. Interestingly, miR-375 overexpression protected MNs from DNA damage-induced apoptosis. Mechanistically, miR-375 may exert this function by targeting p53 (Bhinge et al., 2016; Liu et al., 2013). We show here that p53 and other pro-apoptotic miR-375 predicted targets are upregulated in *FUS* mutant MNs. Notably, spinal MNs of ALS patients have been shown to display higher levels of p53 protein, which could be involved in apoptosis-mediated neuronal death (Martin, 2000; Ranganathan and Bowser, 2010).

In FUS^{P525L} MNs we observed 40%–50% reduction in miR-375 levels. This is strikingly similar to the situation observed by Bhinge et al. (2016) in SMA MNs, in which miR-375 levels were reduced to 40%. Therefore, miR-375 dysregulation represents a common feature between two different MN diseases. While the molecular basis of miR-375 downregulation in SMA MNs remains currently unknown, we propose that ALS mutations causing FUS exclusion from the nucleus impair miR-375 production via a loss-of-function mechanism.

In addition to p53-induced apoptosis, miR-375 dysregulation might have an impact on other crucial pathways. Its decrease in FUS^{P525L} MNs is mirrored by an increase of its target ELAVL4, an RNA-binding protein playing multiple roles in neural development, function, and degeneration (Bronicki and Jasmin, 2013). ELAVL4 regulates the stability and/or localization of several target transcripts. We propose that FUS, through the miR-375/ELAVL4 axis, is hierarchically at the top of a regulatory network with a broader role in the RNA metabolism of MNs.

In conclusion, transcriptome analysis of isogenic FUS^{WT} and FUS^{P525L} *in-vitro*-derived human MNs provided an insight on target genes and pathways altered by ALS mutations in the cell type primarily affected by the disease.

EXPERIMENTAL PROCEDURES

Maintenance and Differentiation of Human iPSCs

Generation and maintenance of iPSC lines is described in Lenzi et al. (2015). The MN differentiation protocol has been modified from Hill et al. (2016). In brief, cells were differentiated in N2B27 medium supplemented with 1 μM all-*trans* retinoic acid (Sigma-Aldrich) and 1 μM SAG (Merck Millipore) for 12 days in the presence of 10 μM SB431542 and 100 nM LDN-193189 (both from Miltenyi Biotec) from day 0 to 6, and 5 μM DAPT and 4 μM SU-5402 (both from Sigma-Aldrich) from day 6 to 12. Cells were sorted at day 12 using a FACSAria III (BD Biosciences) and re-plated on poly-L-ornithine-coated dishes and laminin- coated dishes (both from Sigma-Aldrich) in Neural Medium. The *Hb9*:GFP reporter was stably integrated in the *AAVS1* locus, as described previously (Wainger et al., 2014).

RNA and Protein Analysis

Total RNA, extracted with the Quick-RNA MiniPrep (Zymo Research) and retrotranscribed with SuperScript VILO (Thermo Fisher Scientific) or miScript II RT (QIAGEN), was analyzed by real-time qRT-PCR with SYBR Green PowerUP (Thermo Fisher Scientific) or SYBR Green PCR Master Mix (QIAGEN). For miRNAs 384 array, RNA retrotranscribed using the TaqMan MicroRNA RT Kit was analyzed using the TaqMan Human MicroRNA Array A (Thermo Fisher Scientific). Primers sequences are reported in Table S4. Western blot analysis was carried out using anti-p53 (fl-393; Santa Cruz) and anti-GAPDH (sc-32233) antibodies.

RNA-Seq and Bioinformatics Analysis

Total RNA was sequenced on an Illumina HiSeq 2500 sequencing system using a TruSeq Stranded Total RNA Library Prep Kit with Ribo-Zero treatment (Illumina) or the TruSeq Small RNA Library (Illumina) at the Institute of Applied Genomics (Udine, Italy). An average of about 21 million 125 base pairs long paired-end reads or 17 million 50 base pairs long single-end reads were produced for each sample for RNA-seq or small RNA-seq, respectively. Bioinformatics analysis is described in detail in the Supplemental Experimental Procedures.

RNA-seq raw data have been deposited at the GEO (GEO: GSE94888).

Immunostaining

Immunostaining was performed with anti-Islet-1/2 (1:50, 39.4D5; DSHB) primary antibody and anti-mouse Alexa Fluor 488 (1:250, Thermo Fisher Scientific) goat secondary antibody. Images were acquired with an inverted iX73 microscope (Olympus).

FUS Knockdown and miRNA Mimics Transfection

Differentiating FUS^{WT} iPSCs were transfected at 8 and 10 days with 40 nM anti-FUS siRNAs (SI00070518, QIAGEN) or scramble control siRNAs (1027281, QIAGEN). FUS^{P525L} iPSCs, induced to differentiate into MNs for 14 days and seeded on Matrigel-coated plates, were transfected after 48 hr with 10 nM mirVana miRNA mimics (miR-375-3p MIMAT0000728; Negative Control No. 1 Cat. 4464058; Thermo Fisher Scientific). RNA was collected for real-time qRT-PCR analysis after 48 hr.

ACCESSION NUMBERS

The accession number for the RNA sequencing raw data reported in this paper is GEO: GSE94888.

SUPPLEMENTAL INFORMATION

Supplemental Information includes Supplemental Experimental Procedures, five figures, and four tables and can be found with this article online at https://doi.org/10.1016/j.stemcr.2017.09.004.

AUTHOR CONTRIBUTIONS

A.R. and R.D.S. conceived the project. R.D.S. generated *Hb9*:GFP iPSC lines, set up and optimized MN differentiation and isolation, and collected and analyzed RNA and protein samples. L.S. and V.A. contributed to iPSC culture and differentiation and RNA analysis. A.C. performed the bioinformatics analysis of the RNA-seq. G.P. set up and optimized the fluorescence-activated cell sorting analysis and sorting of MNs. V.d.T. acquired and analyzed microscopy images. A.R. and I.B. coordinated the work and wrote the paper.

ACKNOWLEDGMENTS

We thank Dr. Kevin Eggan (Harvard University) for providing the original MN differentiation protocol and the *Hb9*::GFP reporter construct. We are grateful to members of the Center for Life Nano Science and of the A.R. and I.B. laboratories for helpful discussion. This work was partially supported by AriSLA pilot grant 2016 "StressFUS" to A.R. and AriSLA full grant 2014 "ARCI," ERC-2013 - AdG 340172-MUNCODD, IIT "SEED," Epigen-Epigenomics Flagship Project, Human Frontiers Science Program Award RGP0009/2014, and Fondazione Roma to I.B.

Received: May 9, 2017
Revised: September 5, 2017
Accepted: September 6, 2017
Published: October 5, 2017

REFERENCES

Abdelmohsen, K., Hutchison, E.R., Lee, E.K., Kuwano, Y., Kim, M.M., Masuda, K., Srikantan, S., Subaran, S.S., Marasa, B.S., Mattson, M.P., and Gorospe, M. (2010). miR-375 inhibits differentiation of neurites by lowering HuD levels. Mol. Cell. Biol. *30*, 4197–4210.

Agarwal, V., Bell, G.W., Nam, J.-W., and Bartel, D.P. (2015). Predicting effective microRNA target sites in mammalian mRNAs. Elife *4*. http://dx.doi.org/10.7554/eLife.05005.

Akten, B., Kye, M.J., Hao, L.T., Wertz, M.H., Singh, S., Nie, D., Huang, J., Merianda, T.T., Twiss, J.L., Beattie, C.E., et al. (2011). Interaction of survival of motor neuron (SMN) and HuD proteins with mRNA cpg15 rescues motor neuron axonal deficits. Proc. Natl. Acad. Sci. USA *108*, 10337–10342.

Amin, N.D., Bai, G., Klug, J.R., Bonanomi, D., Pankratz, M.T., Gifford, W.D., Hinckley, C.A., Sternfeld, M.J., Driscoll, S.P., Dominguez, B., et al. (2015). Loss of motoneuron-specific microRNA-218 causes systemic neuromuscular failure. Science *350*, 1525–1529.

Aronica, E., Baas, F., Iyer, A., ten Asbroek, A.L., Morello, G., and Cavallaro, S. (2015). Molecular classification of amyotrophic lateral sclerosis by unsupervised clustering of gene expression in motor cortex. Neurobiol. Dis. *74*, 359–376.

Batra, R., Hutt, K., Vu, A., Rabin, S.J., Baughn, M.W., Libby, R.T., Hoon, S., Ravits, J., and Yeo, G.W. (2016). Gene expression signatures of sporadic ALS motor neuron populations. bioRxiv http://dx.doi.org/10.1101/038448.

Bentmann, E., Haass, C., and Dormann, D. (2013). Stress granules in neurodegeneration - lessons learnt from TAR DNA binding protein of 43 kDa and fused in sarcoma. FEBS J. *280*, 4348–4370.

Bhinge, A., Namboori, S.C., Bithell, A., Soldati, C., Buckley, N.J., and Stanton, L.W. (2016). MiR-375 is essential for human spinal motor neuron development and may be involved in motor neuron degeneration. Stem Cells *34*, 124–134.

Boulting, G.L., Kiskinis, E., Croft, G.F., Amoroso, M.W., Oakley, D.H., Wainger, B.J., Williams, D.J., Kahler, D.J., Yamaki, M., Davidow, L., et al. (2011). A functionally characterized test set of human induced pluripotent stem cells. Nat. Biotechnol. *29*, 279–286.

Bronicki, L.M., and Jasmin, B.J. (2013). Emerging complexity of the HuD/ELAVl4 gene; implications for neuronal development, function, and dysfunction. RNA *19*, 1019–1037.

Buratti, E., De Conti, L., Stuani, C., Romano, M., Baralle, M., and Baralle, F. (2010). Nuclear factor TDP-43 can affect selected microRNA levels. FEBS J. *277*, 2268–2281.

Chou, C.-H., Chang, N.-W., Shrestha, S., Hsu, S.-D., Lin, Y.-L., Lee, W.-H., Yang, C.-D., Hong, H.-C., Wei, T.-Y., Tu, S.-J., et al. (2016). miRTarBase 2016: updates to the experimentally validated miRNA-target interactions database. Nucleic Acids Res. *44*, D239–D247.

Couthouis, J., Hart, M.P., Shorter, J., Dejesus-Hernandez, M., Erion, R., Oristano, R., Liu, A.X., Ramos, D., Jethava, N., Hosangadi, D., et al. (2011). A yeast functional screen predicts new candidate ALS disease genes. Proc. Natl. Acad. Sci. USA *108*, 20881–20890.

D'Andrea, D., Grassi, L., Mazzapioda, M., and Tramontano, A. (2013). FIDEA: a server for the functional interpretation of differential expression analysis. Nucleic Acids Res. *41*, W84–W88.

Di Carlo, V., Grossi, E., Laneve, P., Morlando, M., Dini Modigliani, S., Ballarino, M., Bozzoni, I., and Caffarelli, E. (2013). TDP-43 regulates the microprocessor complex activity during in vitro neuronal differentiation. Mol. Neurobiol. *48*, 952–963.

Dormann, D., and Haass, C. (2011). TDP-43 and FUS: a nuclear affair. Trends Neurosci. *34*, 339–348.

Emde, A., Eitan, C., Liou, L.-L., Libby, R.T., Rivkin, N., Magen, I., Reichenstein, I., Oppenheim, H., Eilam, R., Silvestroni, A., et al. (2015). Dysregulated miRNA biogenesis downstream of cellular stress and ALS-causing mutations: a new mechanism for ALS. EMBO J. *34*, 2633–2651.

Gomes, I., Xiong, W., Miki, T., and Rosner, M.R. (1999). A proline- and glutamine-rich protein promotes apoptosis in neuronal cells. J. Neurochem. *73*, 612–622.

Guio-Vega, G.P., and Forero, D.A. (2017). Functional genomics of candidate genes derived from genome-wide association studies for five common neurological diseases. Int. J. Neurosci. *127*, 118–123.

Haramati, S., Chapnik, E., Sztainberg, Y., Eilam, R., Zwang, R., Gershoni, N., McGlinn, E., Heiser, P.W., Wills, A.-M., Wirguin, I., et al. (2010). miRNA malfunction causes spinal motor neuron disease. Proc. Natl. Acad. Sci. USA *107*, 13111–13116.

Hill, S.J., Mordes, D.A., Cameron, L.A., Neuberg, D.S., Landini, S., Eggan, K., and Livingston, D.M. (2016). Two familial ALS proteins function in prevention/repair of transcription-associated DNA damage. Proc. Natl. Acad. Sci. USA *113*, E7701–E7709.

Ichiyanagi, N., Fujimori, K., Yano, M., Ishihara-Fujisaki, C., Sone, T., Akiyama, T., Okada, Y., Akamatsu, W., Matsumoto, T., Ishikawa, M., et al. (2016). Establishment of in vitro fus-associated familial amyotrophic lateral sclerosis model using human induced pluripotent stem cells. Stem Cell Reports *6*, 496–510.

Kapeli, K., Pratt, G.A., Vu, A.Q., Hutt, K.R., Martinez, F.J., Sundararaman, B., Batra, R., Freese, P., Lambert, N.J., Huelga, S.C., et al. (2016). Distinct and shared functions of ALS-associated proteins TDP-43, FUS and TAF15 revealed by multisystem analyses. Nat. Commun. *7*, 12143.

Kawahara, Y., and Mieda-Sato, A. (2012). TDP-43 promotes microRNA biogenesis as a component of the Drosha and Dicer complexes. Proc. Natl. Acad. Sci. USA *109*, 3347–3352.

Kino, Y., Washizu, C., Kurosawa, M., Yamada, M., Miyazaki, H., Akagi, T., Hashikawa, T., Doi, H., Takumi, T., Hicks, G.G., et al. (2015). FUS/TLS deficiency causes behavioral and pathological abnormalities distinct from amyotrophic lateral sclerosis. Acta Neuropathol. Commun. *3*, 24.

Kiskinis, E., Sandoe, J., Williams, L.A., Boulting, G.L., Moccia, R., Wainger, B.J., Han, S., Peng, T., Thams, S., Mikkilineni, S., et al. (2014). Pathways disrupted in human ALS motor neurons identified through genetic correction of mutant SOD1. Cell Stem Cell *14*, 781–795.

Kong, Y., Liang, X., Liu, L., Zhang, D., Wan, C., Gan, Z., and Yuan, L. (2015). High throughput sequencing identifies microRNAs mediating α-synuclein toxicity by targeting neuroactive-ligand receptor interaction pathway in early stage of drosophila Parkinson's disease model. PLoS One *10*, e0137432.

Kotni, M.K., Zhao, M., and Wei, D.-Q. (2016). Gene expression profiles and protein-protein interaction networks in amyotrophic lateral sclerosis patients with C9orf72 mutation. Orphanet J. Rare Dis. *11*, 148.

Kwiatkowski, T.J., Bosco, D.A., Leclerc, A.L., Tamrazian, E., Vanderburg, C.R., Russ, C., Davis, A., Gilchrist, J., Kasarskis, E.J., Munsat, T., et al. (2009). Mutations in the FUS/TLS gene on chromosome 16 cause familial amyotrophic lateral sclerosis. Science *323*, 1205–1208.

Kye, M.J., and Gonçalves, I.D.C.G. (2014). The role of miRNA in motor neuron disease. Front. Cell. Neurosci. *8*, 15.

Lagier-Tourenne, C., Polymenidou, M., Hutt, K.R., Vu, A.Q., Baughn, M., Huelga, S.C., Clutario, K.M., Ling, S.-C., Liang, T.Y., Mazur, C., et al. (2012). Divergent roles of ALS-linked proteins FUS/TLS and TDP-43 intersect in processing long pre-mRNAs. Nat. Neurosci. *15*, 1488–1497.

Lenzi, J., De Santis, R., de Turris, V., Morlando, M., Laneve, P., Calvo, A., Caliendo, V., Chiò, A., Rosa, A., and Bozzoni, I. (2015). ALS mutant FUS proteins are recruited into stress granules in induced pluripotent stem cells (iPSCs) derived motoneurons. Dis. Model. Mech. *8*, 755–766.

Lenzi, J., Pagani, F., De Santis, R., Limatola, C., Bozzoni, I., Di Angelantonio, S., and Rosa, A. (2016). Differentiation of control and ALS mutant human iPSCs into functional skeletal muscle cells, a tool for the study of neuromuscular diseases. Stem Cell Res. *17*, 140–147.

Ling, S.-C., Polymenidou, M., and Cleveland, D.W. (2013). Converging mechanisms in ALS and FTD: disrupted RNA and protein homeostasis. Neuron *79*, 416–438.

Liu, Y., Xing, R., Zhang, X., Dong, W., Zhang, J., Yan, Z., Li, W., Cui, J., and Lu, Y. (2013). miR-375 targets the p53 gene to regulate cellular response to ionizing radiation and etoposide in gastric cancer cells. DNA Repair (Amst) *12*, 741–750.

Martin, L.J. (2000). p53 is abnormally elevated and active in the CNS of patients with amyotrophic lateral sclerosis. Neurobiol. Dis. *7*, 613–622.

Morlando, M., Dini Modigliani, S., Torrelli, G., Rosa, A., Di Carlo, V., Caffarelli, E., and Bozzoni, I. (2012). FUS stimulates microRNA biogenesis by facilitating co-transcriptional Drosha recruitment. EMBO J. *31*, 4502–4510.

Neumann, M., Bentmann, E., Dormann, D., Jawaid, A., Dejesus-Hernandez, M., Ansorge, O., Roeber, S., Kretzschmar, H.A., Munoz, D.G., Kusaka, H., et al. (2011). FET proteins TAF15 and EWS are selective markers that distinguish FTLD with FUS pathology from amyotrophic lateral sclerosis with FUS mutations. Brain *134*, 2595–2609.

Orozco, D., and Edbauer, D. (2013). FUS-mediated alternative splicing in the nervous system: consequences for ALS and FTLD. J. Mol. Med. *91*, 1343–1354.

Ranganathan, S., and Bowser, R. (2010). p53 and cell cycle proteins participate in spinal motor neuron cell death in ALS. Open Pathol. J. *4*, 11–22.

Renton, A.E., Chiò, A., and Traynor, B.J. (2014). State of play in amyotrophic lateral sclerosis genetics. Nat. Neurosci. *17*, 17–23.

Sances, S., Bruijn, L.I., Chandran, S., Eggan, K., Ho, R., Klim, J.R., Livesey, M.R., Lowry, E., Macklis, J.D., Rushton, D., et al. (2016). Modeling ALS with motor neurons derived from human induced pluripotent stem cells. Nat. Neurosci. *16*, 542–553.

Scekic-Zahirovic, J., Sendscheid, O., El Oussini, H., Jambeau, M., Sun, Y., Mersmann, S., Wagner, M., Dieterlé, S., Sinniger, J., Dirrig-Grosch, S., et al. (2016). Toxic gain of function from mutant FUS protein is crucial to trigger cell autonomous motor neuron loss. EMBO J. *35*, 1077–1097.

Tollervey, J.R., Curk, T., Rogelj, B., Briese, M., Cereda, M., Kayikci, M., König, J., Hortobágyi, T., Nishimura, A.L., Župunski, V., et al. (2011). Characterizing the RNA targets and position-dependent splicing regulation by TDP-43. Nat. Neurosci. *14*, 452–458.

Vance, C., Rogelj, B., Hortobágyi, T., De Vos, K.J., Nishimura, A.L., Sreedharan, J., Hu, X., Smith, B., Ruddy, D., Wright, P., et al. (2009). Mutations in FUS, an RNA processing protein, cause familial amyotrophic lateral sclerosis type 6. Science *323*, 1208–1211.

Vance, C., Scotter, E.L., Nishimura, A.L., Troakes, C., Mitchell, J.C., Kathe, C., Urwin, H., Manser, C., Miller, C.C., Hortobágyi, T., et al. (2013). ALS mutant FUS disrupts nuclear localization and sequesters wild-type FUS within cytoplasmic stress granules. Hum. Mol. Genet. *22*, 2676–2688.

Wainger, B.J., Kiskinis, E., Mellin, C., Wiskow, O., Han, S.S.W., Sandoe, J., Perez, N.P., Williams, L.A., Lee, S., Boulting, G., et al. (2014). Intrinsic membrane hyperexcitability of amyotrophic lateral sclerosis patient-derived motor neurons. Cell Rep. *7*, 1–11.

Zhao, L.Y., Niu, Y., Santiago, A., Liu, J., Albert, S.H., Robertson, K.D., and Liao, D. (2006). An EBF3-mediated transcriptional program that induces cell cycle arrest and apoptosis. Cancer Res. *66*, 9445–9452.